



GEOPOLYMER CONCRETE EVALUATIONS USING A VARIETY OF TECHNIQUES

GEETHIKA G PILLAI, TEENA JOY

Department of Civil Engineering, Indira Gandhi Institute Of Engineering And Technology,
Nellikuzhi P.O, Kothamangalam, Ernakulam (Dist) Pincode 686691

Abstract

Research on the alkali activation of waste materials, such as fly ash, has gained significance because of the potential to produce cost-effective and environmentally friendly cement-like building materials. This study describes the process of activating a fly ash using a very alkaline solution. The solutions produced with NaOH and Na₂SiO₃ have the common trait of having a very high concentration of OH⁻ ions. Due to their strong and mostly non-crystalline microstructure, materials containing latent hydraulic active chemicals activated by alkalis, such as fly ash, are classified as "chemically bonded products." The polymerization of fly ashes results in the formation of a novel kind of eco-friendly concrete, which has an amorphous nature with a few crystalline phases present in smaller quantities.

Keywords: Alkaline liquid, Fly ash, Geopolymer concrete, Scanning electron microscopy (SEM), X-ray diffraction (XRD)

1. Introduction

Geopolymer concrete, which incorporates waste material rich in silica (Si) and alumina (Al) like fly ash, is a favourable substitute due to its significantly reduced greenhouse gas emissions in comparison to ordinary Portland cement (OPC) concrete. The alkaline activators in geopolymer concrete initiate the formation of a gel by stimulating the silica and alumina found in the source materials. The geopolymer gel acts as a binder, joining together the loose aggregates and any remaining un-reacted components in the mixture, resulting in the formation of geopolymer concrete. The chemical process involved in the synthesis of geopolymer binders differs significantly from that of OPC concrete. The emergence of sophisticated experimental methods, such as SEM analysis and X-ray Diffraction method, is used to elucidate crucial features of the structure and morphology of these novel materials. A Scanning Electron Microscope (SEM) is an electron microscope that generates pictures of a material by scanning it with a concentrated stream of electrons. The electrons engage in interactions with electrons inside the sample, generating diverse signals that are detectable and may include valuable information on the surface topography and composition of the sample. The electron beam is typically moved in a raster scan pattern, and the location of the beam is coupled with the acquired signal to create a picture. Scanning Electron Microscopy (SEM) is capable of achieving resolutions superior to 1 nanometer. Specimens may be examined in both high vacuum and low vacuum conditions. Additionally, environmental SEM specimens can be observed in a wet state. X-ray scattering techniques include a group of non-invasive analytical methods that provide insights into the crystal structure, chemical content, and physical characteristics of materials and thin films. These



approaches rely on the observation of the dispersed intensity of an X-ray beam as it interacts with a material, taking into account factors such as incident and scattered angle, polarisation, and wavelength or energy. An X-Ray Diffraction (XRD) examination was performed to determine the silica phase of the geopolymer concrete sample. Initially, the specimens were examined using an X-ray diffractometer equipped with $\text{CuK}\alpha$ radiation at 40kV / 20 mA. The scanning parameters were set as follows: CPS = 1 k, width 2.5, speed 2° / min, and a scanning angle of 2 Theta ranging from 10° to 80° . X-ray diffraction involves the scattering of X-rays by atoms, resulting in a pattern that reveals the lattice spacing of the elements in the specimen being analysed. When the X-rays are in phase, they will exhibit constructive interference, resulting in the formation of a peak in the X-ray diffraction pattern at a certain wavelength. The X-ray wavelength is measured over a broad variety of angles, and subsequently the material spacing is determined.

2. Experimental

The microstructural studies were conducted using fly ash and geopolymer concrete.

A Scanning Electron Microscope (SEM) uses Back-Scattered Electrons (BSE), which are electrons in the beam that are reflected off the sample due to elastic scattering. Backscattered electrons (BSEs) are often used in analytical scanning electron microscopy (SEM) in conjunction with spectra generated from characteristic X-rays. This is due to the fact that the strength of the BSE signal is closely correlated with the atomic number (Z) of the specimen. Images obtained using backscattered electron (BSE) imaging techniques may provide valuable insights into the spatial distribution of various components inside the sample. For further analysis, the fly ash sample, OPC, and GPC samples, which had previously undergone compressive strength testing at 28 days, were fragmented into smaller specimens and ground into a fine powder. The resulting powder was then securely stored in air-tight zip lock bags. Subsequently, the specimens were meticulously processed and subjected to analysis using a Scanning Electron Microscope (SEM) to evaluate the microstructure in a qualitative manner. The scanning electron microscope is an invaluable instrument for observing the microscopic structural evolution of the fly ash and the geopolymer concrete matrix specimen.

X-ray diffraction is a method used to qualitatively determine the elements and compounds contained in a sample. An X-ray diffractometer was used to analyse the specimen samples of low calcium fly ash and geopolymer concrete. A minute quantity of specimen material, in the form of powder, was placed into an aluminium sample container and the surface was levelled. The specimen was thereafter inserted into the X-ray diffractometer and examined within the range of 10° to 80° in terms of 2 Theta angles. The analysis was conducted with a precision of 0.04 degrees and timed for a duration of 3 seconds. The X-ray diffraction examination revealed the presence of many minerals in the samples. The peak intensities of each sample were analysed based on the individual angles obtained from the database.

3. Results and Discussions

Figures 1 show the scanning electron microscope (SEM) pictures of fly ash powder at various magnifications. Figure 1(a) shows a micrograph displaying an enlarged picture of fly ash at a magnification of 200. The display exhibits a sequence of spherical and glassy particles with sizes ranging from 9 μm to 82 μm . The scale bar measures 100 micrometres. Figure 1(b) is a micrograph displaying a highly enlarged picture of fly ash at a magnification of 500x. The display indicates the size of the fly ash particles, which vary between 4 μm and 35 μm . The particles have a spherical form and the scale bar measures 50 μm . Figure 1(c) is a micrograph showing a highly enlarged picture of fly ash at a magnification of 700x. The statement denotes the presence of fly ash particles that are spherical in form and have a size ranging from 2.5 μm to 32.5 μm . The scale bar measures 20 micrometres. Furthermore, Figure 1(d) displays a micrograph that showcases a magnified picture of the fly ash at a greater level of magnification, namely 1000x magnification. The image displays the dimensions of fly ash particles, namely their diameter, which varies between 7.5 μm and 35 μm . The scale bar in the image represents a length of 10 μm .

From micrographs 1(a) to 1(d), SEM pictures show the original fly ash's morphology. This fly ash contains spherical and vitreous particles ranging from 7.5 to 35 μm in size. Some fly ash spheres may include smaller particles since they are hollow. Fly ash's spherical shape makes it easy to create a simple conceptual mix that describes its alkali activation. Fly ash activates nearly completely, creating a thick paste.

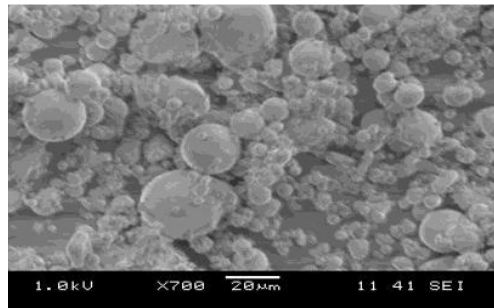
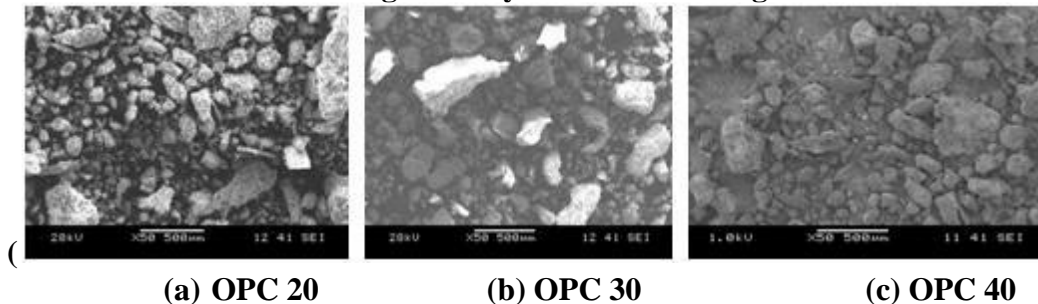


Figure 1 Fly Ash with 700 Magnification



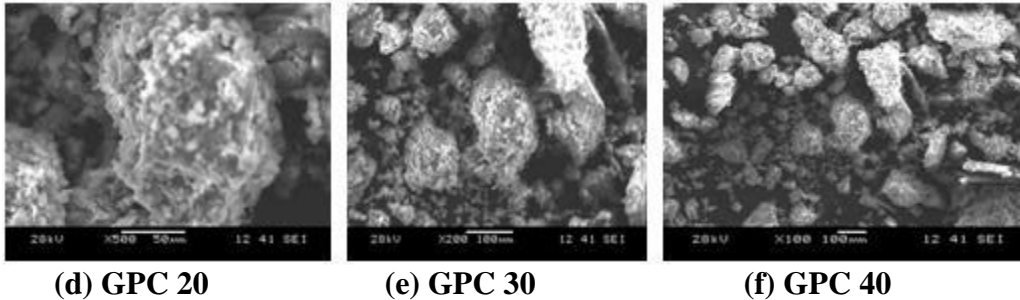


Figure 2 SEM Images of OPC and GPC for Various Grades

Figure 2 shows basic port land cement concrete and geopolymer concrete microstructures for M20, M30, and M40 grades. The scale bar and magnification factor of each OPC and GPC grade are also shown. Figure 2 (a) shows a 50-magnification SEM image of grade 20 OPC. The particles were irregularly shaped, with lateral dimensions ranging from 100 to 400 μm and lengths from 400 to 1200 μm . The scale bar measures 500 μm . More voids separate these particles. A 50-magnification micrograph of grade 30 OPC is shown in Figure 2 (b). The picture exhibits rectangular and irregular particles. The particle sizes ranged from 20 to 145 μm in width and 62 to 790 μm in length. The scale bar measures 500 μm . The OPC 30 micrograph shows less thick concrete paste. It's somewhat permeable.

An OPC grade 40 micrograph at 50 magnification is shown in Figure 2(c). Image shows irregular particle. The particle sizes ranged from 15 to 150 μm in diameter. The scale bar measures 500 μm . The OPC 40 micrograph shows loosely packed concrete paste. Figure 2 (d) shows a 500-magnification SEM picture of grade 20 GPC. The picture shows that fly ash polymerizes alkaline liquids to generate a thick coating of particles. The particle sizes ranged from 15 to 160 μm in diameter. The scale bar is 50 μm . GPC 20's micrograph shows thick concrete paste.

Figure 2 (e) shows a 200-magnification SEM image of grade 30 GPC. The picture depicts viscous particles forming a thick threaded paste cluster. The particle sizes ranged from 20 to 170 μm in diameter. The scale bar is 100 μm . The GPC 30 micrograph shows more tightly packed concrete paste than GPC 20. Figure 2 (f) shows a 100-magnification micrograph of grade 40 GPC. The picture reveals irregularly formed, compact, viscous particles. The particle sizes ranged from 15 to 140 μm in width. The scale bar measures 500 μm . OPC 40 concrete paste is denser and closer than GPC 20 and GPC 30 grade mixes, according to the micrograph.

Geopolymer concrete particles are uneven yet compact, as seen in Figure 2. This geopolymer concrete shows the continuity of the reaction product mass as a layer of viscous fluid frozen, demonstrating full polymerization. The activation reaction rate and chemical composition of these products rely on fly ash particle size distribution, mineral content, and activator penetration. The specimen is fly ash paste activated by sodium silicate and sodium hydroxide. Thermally curing at 900C for 72 hours follows. A homogenous and unshaped microstructure is created in geopolymer concrete.

Low calcium fly ash X-ray diffraction pattern is shown in Figure 3. In this approach, the 2θ angle is plotted on the abscissa and mineral intensity along the ordinate. The graph displays the 2θ angle from 0 to 60. Counts measure intensity. XRD was used to identify the sample's silica phase. This guaranteed qualitative element and compound determination in the sample. The X-ray diffraction data shows many minerals in the sample. Silica, calcium, alumina, and oxides were found. This fly ash sample included low-intensity Quartz. The basic lattice and hexagonal crystalline system. Mineral molecular weight was 60.08.

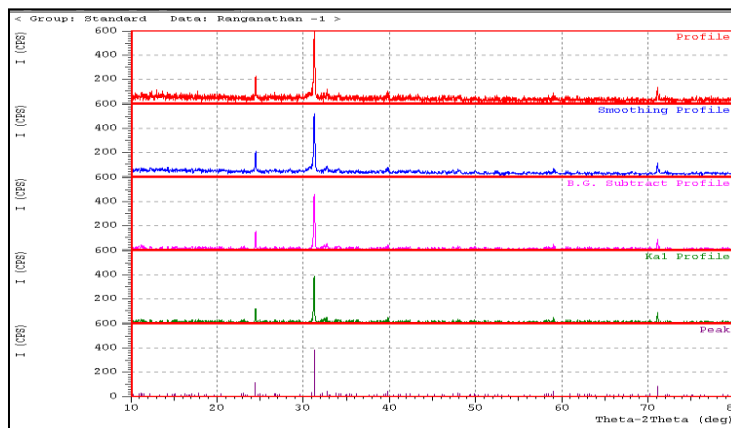


Figure 3: X-Ray Diffraction Pattern of Low Calcium Fly Ash

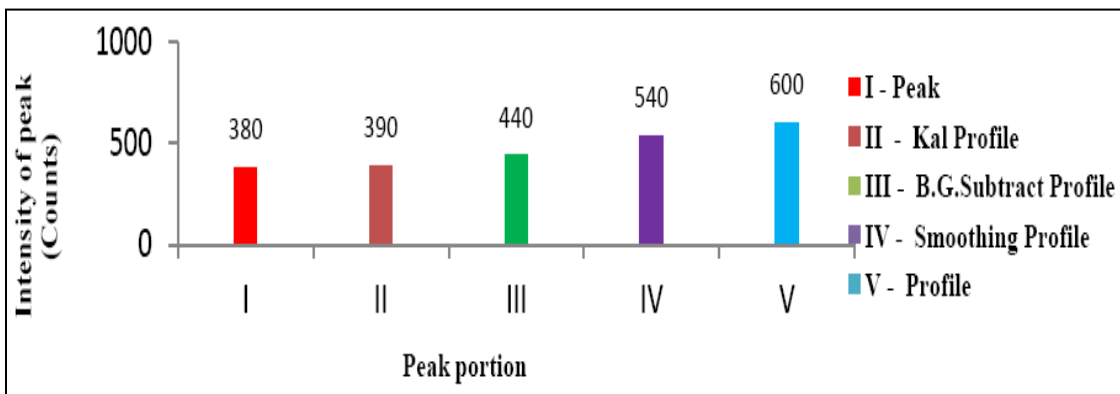


Figure 4: Intensity of Silicon Oxides in Fly Ash Sample

Figure 4 plots fly ash sample silicon oxide intensity from XRD graphs. Figure 4 shows that fly ash silicon oxide concentration ranges from 380 to 600 counts. Silicon oxide intensity is 60% higher than I-peak intensity in the V-profile. V-profile intensities are 55% and 37% greater than II-Kal and III-B. G. remove profiles. V-profile intensity is 11% higher than IV-smoothing profile intensity. These results show that silicon content intensity grew progressively and peaked at the profile. The geopolymer concrete powder X-ray diffraction pattern is shown in Figure 5. It verifies that the peak indicates sodium hydroxide and sodium silicate in concrete powder. Activating fly ash with sodium silicate and sodium hydroxide solutions did not produce crystalline phase, according to X-ray data.

Thus, XRD showed amorphous components in all samples.

Geopolymer concrete sample X-ray Diffraction pattern is shown in Figure 5. The graph has a 2θ angle range of 10° to 80° and an intensity range of 0 to 150 counts. NaOH was more crystalline in this graph. This crystal system was orthorhombic. Lattice was end-centered. Mineral has a molecular weight of 40.00, CD = 131.47, and $D_x = 2.021$. Crystalline NaOH was seen at 2θ angles of 31° , 34° , and 37° . These peaks indicated crystalline sodium hydroxide, whereas numerous other tiny peaks indicated various oxide chemicals in the sample.

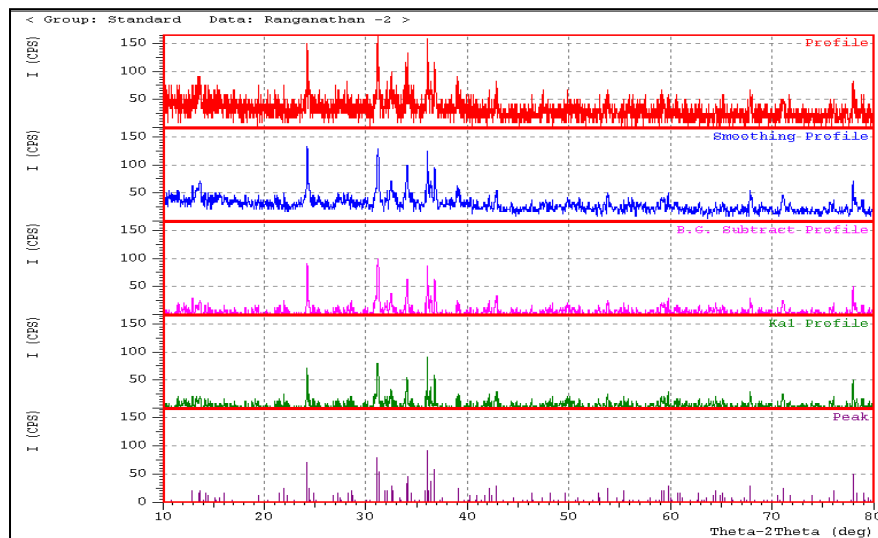


Figure 5: X-Ray Diffraction Pattern of Geopolymer Concrete

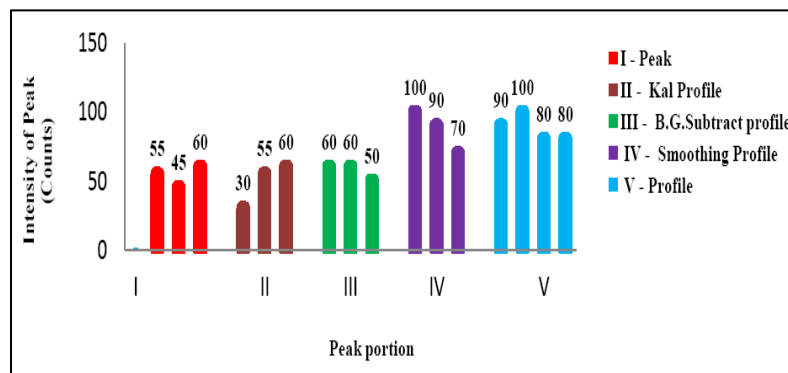


Figure 6: Intensity of Sodium Hydroxide in Geopolymer Concrete Sample

Figure 6 plots sodium hydroxide intensity of geopolymer concrete sample from XRD graphs. Figure 6 shows that geopolymer concrete has 30–100 sodium hydroxide counts. The V-profile shows silicon oxide intensity 70% higher than the I-peak. V-profile intensities are 80% and 60% greater than II-Kal and III-B. G. remove profiles. The V-profile intensity is 4% higher than IV-smoothing. These data

show that sodium hydroxide content intensity rose exclusively in IV-smoothing profile and V-profile sections and peaked at profile portion.

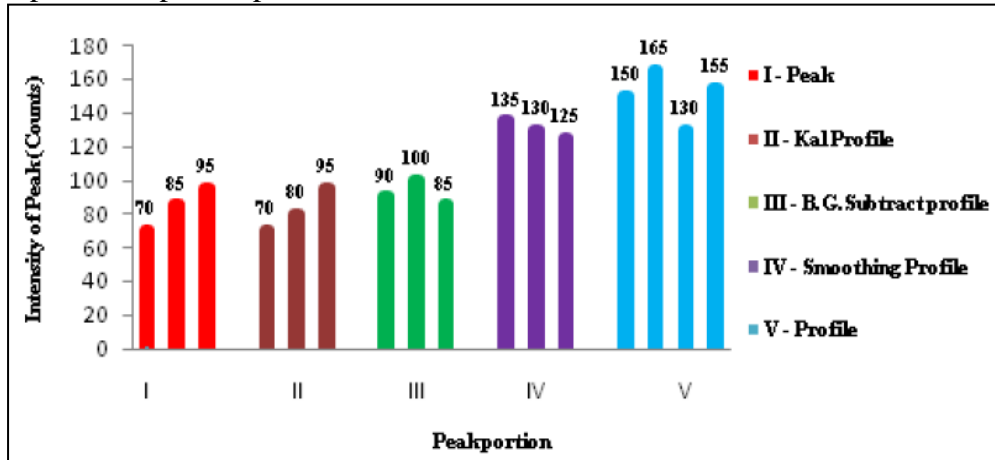


Figure 7: Intensity of Sodium Silicate in Geopolymer Concrete Sample

Figure 7 plots sodium silicate intensity from XRD graphs of geopolymer concrete samples. This shows that geopolymer concrete has 70–165 sodium silicate levels. Silicon oxide intensity is 90% higher in the V-profile than in the I-peak. V-profile intensities are 78% and 72% greater than II-Kal and III-B. G. remove profiles. The V-profile intensity is 21% higher than IV-smoothing. These findings show that sodium silicate content intensity rose exclusively in IV-smoothing profile and V-profile regions and peaked in the profile portion.

4. Conclusion

The following findings were derived from experiments:

The SEM diagram clearly shows the micro structural variations between fly ash and geopolymer concrete. Fly ash particles are spherical and vary in diameter from 10 to 200 micrometres. The thick SEM picture of fly ash suggests effective alkali activation. According to SEM images, the microstructure of conventional Portland cement concrete is porous and not dense. Geopolymer concrete's SEM picture shows a completely formed and compact microstructure, proving polymerization. XRD investigation reveals silicon oxide in fly ash at 32° 2θ angle, with 600 counts. In geopolymer concrete samples, sodium hydroxide chemical intensity is 100 counts at 34° and 36° 2θ angles. The sodium silicate in geopolymer concrete samples peaks at 165 counts at a 2θ angle of 32° .

5. References

- [1]. Djwantoro Hardjito and Steenie, E. Wallah, “Development of Fly ash-based Geopolymer Concrete”, ACI Materials Journal, 101(6), 2004, 467-472
- [2]. Davidovits, J. “Global Warming Impact on the Cement and Aggregates Industries”, World Resource Review, 6(2), 1994, 263-278



-
- [3]. Douglas C. Comrie, John H. Paterson and Douglas J. Ritcey, "Applications of Geopolymer Technology to its stabilization", D. Comrie consulting Ltd, 120 Traders Boulevard east, Suite 209, Mississauga, Ontario, L4Z 2H7, 1998, 161-165
- [4]. Fernandez Jimenez, A., Palomo, A. and Criado, M., "Microstructure development of alkali-activated fly ash cement: a descriptive model", Cement and Concrete Research, 34(6), 2004, 1204-1209
- [5]. Fernandez Jimenez, A.M. and De La Torre, A.G., "Quantitative determination of Phases in the alkali activation of fly ash Part I", Potential Ash Reactivity, Fuel, 85(5-6), 2006, 625-634
- [6]. Frantisek Skvara, Tomas Jilek and Lubomir Kopecky, "Geopolymer materials based on Fly ash", Ceramics Silika, 49(3), 2005, 195-204
- [7]. Frantisek Skvara, "Alkali activated materials or Geopolymers", Lecture notes, Department of Glass and Ceramics, Institute of Chemical Technology, Prague, 2007, 173-177
- [8]. Hassan A, Arif M, Shariq M. A review of properties and behaviour of reinforced geopolymer concrete structural elements-A clean technology option for sustainable development. Journal of Cleaner Production. 2020 Feb 1;245:118762. Das SK, Mishra J, Mustakim SM. An overview of current research trends in geopolymer concrete. Int. Res. J. Eng. Technol. 2018 Nov;5(11):376-81.
- [9]. Nurrudin MF, Sani H, Mohammed BS, Shaaban I. Methods of curing geopolymer concrete: A review. International Journal of Advanced and Applied Sciences. 2018 Jan 1;5(1):31-6.
- [10]. Wasim M, Ngo TD, Law D. A state-of-the-art review on the durability of geopolymer concrete for sustainable structures and infrastructure. Construction and Building Materials. 2021 Jul 12;291:123381.
- [11]. Raijiwala, D.B. and Patil, H.S. "Geopolymer concrete: A concrete of next decade", Journal of Engineering Research and Studies, 2(2), 2011, 19-25
- [12]. Mohammed AA, Ahmed HU, Mosavi A. Survey of mechanical properties of geopolymer concrete: a comprehensive review and data analysis. Materials. 2021 Aug 20;14(16):4690.